Zonal-mean temperature variations inferred from SABER measurements on TIMED compared with UARS observations

Frank T. Huang,[1] Hans G. Mayr,[2] Carl A. Reber,[2] James Russell,[3] Marty Mlynczak,[4] and John Mengel[5]

Received 13 September 2005; revised 8 March 2006; accepted 12 April 2006; published 24 August 2006.

[1] In the zonal mean meridional winds of the upper mesosphere, oscillations with periods between 1 and 4 months have been inferred from UARS measurements and independently predicted with the Numerical Spectral Model (NSM). The wind oscillations tend to be confined to low latitudes and appear to be driven, at least in part, by wave-mean-flow interactions. Winds across the equator should generate, due to dynamical heating and cooling, temperature oscillations with opposite phase in the two hemispheres. Investigating this phenomenon, we have analyzed SABER temperatures from TIMED in the altitude range between 55 and 95 km to delineate with an empirical model, the year-long variability of the migrating tides and zonal mean components. The inferred seasonal variations of the diurnal tide, characterized by amplitude maxima near equinox, are in substantial agreement with UARS observations and results from the NSM. For the zonal mean, the dominant seasonal variations in the SABER temperatures, with annual (12 months) and semiannual (6 months) periodicities, agree well with those derived from UARS measurements. The intraseasonal variations with periods between 2 and 4 months have amplitudes close to 2 K, almost half as large as those for the dominant seasonal variations. Their amplitudes are in qualitative agreement with the corresponding values inferred from UARS during different years. The SABER and UARS temperature variations reveal pronounced hemispherical asymmetries, consistent with meridional wind oscillations across the equator. The phase of the semiannual temperature oscillations from the NSM agrees with the observations from UARS and SABER. However, the amplitudes are systematically smaller, which may indicate that planetary waves are more important than is allowed for in the model. For the shorter-period intraseasonal variations, which can be generated by gravity wave drag, the model results are generally in better agreement with the observations.

Citation: Huang, F. T., H. G. Mayr, C. A. Reber, J. Russell, M. Mlynczak, and J. Mengel (2006), Zonal-mean temperature variations inferred from SABER measurements on TIMED compared with UARS observations, *J. Geophys. Res.*, *111*, A10S07, doi:10.1029/2005JA011427.

1. Introduction

[2] Recent results derived independently from satellite measurements in the upper mesosphere and from the Numerical Spectral Model (NSM) indicate the existence of persistent oscillations in the zonal-mean meridional winds across the equator. Largely confined to low latitudes, the oscillations have periods between 1 and 4 months and amplitudes of a few m/s. The model results were reported by *Mayr et al.* [2003], and the empirical results [*Huang et al.*, 2005; *Huang and Reber*, 2003] were based on measurements from the High Resolution Doppler Imager (HRDI) [*Hays et al.*, 1993] on the Upper Atmosphere Research Satellite (UARS) [*Reber*, 1993]. The reported observations were restricted to 95 km, where HRDI makes both daytime and nighttime measurements to resolve also the large diurnal variations that need to be accounted for in the analysis. *Lieberman* [1998] has presented winds based on HRDI data but for the zonal component. Using ground-based radar data, *Eckermann et al.* [1997] detected intraseasonal winds over Christmas Island (2°N, 157°W). While the radar measurements were obtained from one longitude, our data and model results represent zonal means.

[3] In the model the meridional wind oscillations were generated primarily by gravity waves propagating in the north/south direction. Through dynamical heating and cooling, such oscillations should produce temperature variations in the northern and southern hemispheres that tend to be out of phase. On the basis of data from the Microwave Limb

[1]Creative Computing Solutions Inc., Rockville, Maryland, USA.
[2]NASA Goddard Space Flight Center, Greenbelt, Maryland, USA.
[3]Center for Atmospheric Sciences, Hampton University, Hampton, Virginia, USA.
[4]NASA Langley Research Center, Hampton, Virginia, USA.
[5]Science Systems and Applications, Lanham, Maryland, USA.

0148-0227/06/2005JA011427

Sounder (MLS) [*Barath et al.*, 1993] and the Cryogenic Limb Array Etalon Spectrometer (CLAES) [*Roche et al.*, 1993], both on the UARS spacecraft, *Huang et al.* [2005] reported temperature variations with periods between 1 and 4 months that indeed display this kind of hemispherical asymmetry. However, MLS and CLAES did not measure temperatures much above 55 km, which is well below the 95 km altitude of the HRDI wind data.

[4] For the present study, we analyze the temperature measurements from the Sounding of the Atmosphere using Broadband Emission Radiometry instrument (SABER) [*Russell et al.*, 1999] on the Thermosphere-Ionosphere-Mesosphere-Energetics and Dynamics (TIMED) satellite, which provides data over a large altitude range, from the stratosphere into the thermosphere. We compare the TIMED data with the corresponding temperature results obtained from UARS and from the NSM. In section 2.1, we describe the measurements, the sampling issues, and the analysis algorithm. Since the data are only sampled essentially at two local solar times during a given day for a given latitude, estimates of the zonal mean (average of the data around a latitude circle) can be biased by the diurnal variations that characterize tidal phenomena. In order to estimate the variations for the zonal mean, the diurnal variations thus need to be estimated as well [e.g., *Beig et al.*, 2003; *Forbes et al.*, 1997]. In section 2.2, we briefly describe the NSM. In section 3 we present the empirical results for the zonal mean temperatures and show also briefly the tidal amplitudes that are estimated with the same algorithm. Although our focus is on the higher harmonics (periods of 4 months and less), we also present the results for the annual and semiannual components. Previous studies [e.g., *Fleming et al.*, 1988, 1990; *Remsberg et al.*, 2002] concentrated mainly on the annual mean and the annual and semiannual harmonics but did not address much the higher harmonics.

2. Data Analysis and Model

2.1. Data Analysis

[5] To analyze the behavior of zonal mean temperature variations at different latitudes, the Fourier harmonics are derived for the annual cycle (with day of year as independent variable). In the following, we first discuss the data sampling properties and the resulting caveats that need to be considered for the analysis.

2.1.1. Satellite Measurements and Sampling

[6] The temperature measurements come from SABER on TIMED and from MLS on UARS. The SABER and MLS instruments measure radiation as they view the Earth's limb, and the kinetic temperatures are retrieved by applying radiative transfer analysis. The data are sampled at different latitudes because of the north/south motion of the satellites, and different longitudes are sampled due to the rotation of the Earth relative to the orbital plane. Since it takes up to 1 day to sample the data over the globe, the measurements are not obtained simultaneously.

[7] The SABER project supplies level 2 data, which represent the measurements at the footprints of the instrument as a function of space and time (not necessarily at regular intervals). We have interpolated the data to fixed altitude surfaces and latitudes. They were then averaged over longitude for the analysis. MLS retrieves temperatures at standard UARS pressure surfaces. The highest altitude at which data are retrieved is 0.46 hPa, which is approximately 55 km. SABER provides data at altitude intervals of less than 0.5 km, and we interpolate them to 55 km for comparison with MLS. The resolution of SABER is about 2 km, while that of MLS is about twice that large. Since we are not making quantitative comparisons, the altitude difference is within the resolution of MLS and SABER, and, in any event, the MLS and SABER measurements were made about 10 years apart.

[8] At any given day and irrespective of longitude, satellites usually sample the data at only two local solar times around a latitude circle, one for the orbit-ascending mode, and one for the descending mode. For Sun-synchronous satellites, the two local times remain the same throughout the mission. Unlike Sun-synchronous satellites, the orbital planes of TIMED and UARS precess slowly (owing to the respective orbital inclinations of 74° and 57°), such that from day to day, for a given latitude and orbital mode (ascending or descending), the local times of the measurements decrease by about 12 and 20 min, respectively. Using both orbital modes, it takes 60 days for TIMED to sample the full range of local times (and 36 days for UARS). When taking the average of the data over longitudes (around a given latitude circle) for a given day, they represent essentially only one local time for each of the two orbital modes. The inferred values of the zonal mean are thus biased by the diurnal variations associated with tides. In the mesosphere and thermosphere, tidal winds can dominate with amplitudes approaching 100 m/s, and tidal temperature amplitudes can reach 20°K. The diurnal variations thus need to be considered in conjunction with the variations of the zonal mean component [e.g., *Beig et al.*, 2003].

[9] In Figure 1 we show the 95 km SABER temperature data (°K) averaged over longitude, plotted as a function of day of year (2003) at the equator (Figure 1a) and at 16°N (Figure 1b) latitude. The solid and dashed lines represent the ascending and descending mode data, respectively, corresponding to the two different local times (LST) for each day. (As stated above, it takes 60 days to sample the data over the full range of local times.) The asterisks represent the estimated zonal means using our algorithm, which is described in the next section. At the equator (Figure 1a), differences between respective modes (different local times) reflect the large tidal amplitudes of almost 20°K. At 16°N (Figure 1b), the differences between ascending and descending mode data are relatively small, reflecting the smaller tidal amplitudes at this latitude. The zonal mean component is thus readily discernable, being reasonably approximated by the average of the ascending and descending mode data. Obviously this is not true for the equator, with large tidal variability, where the average of ascending and descending mode data may not provide a good estimate for the zonal mean.

[10] To overcome some of the limitations imposed by the asynoptic sampling, the analysis uses an algorithm that estimates the diurnal (including semidiurnal) variations and the zonal-mean values together, as described in the next section (section 2.1.2). For the analysis presented here, the data are averaged in longitude over a latitude circle. The resulting diurnal variations thus describe the migrating

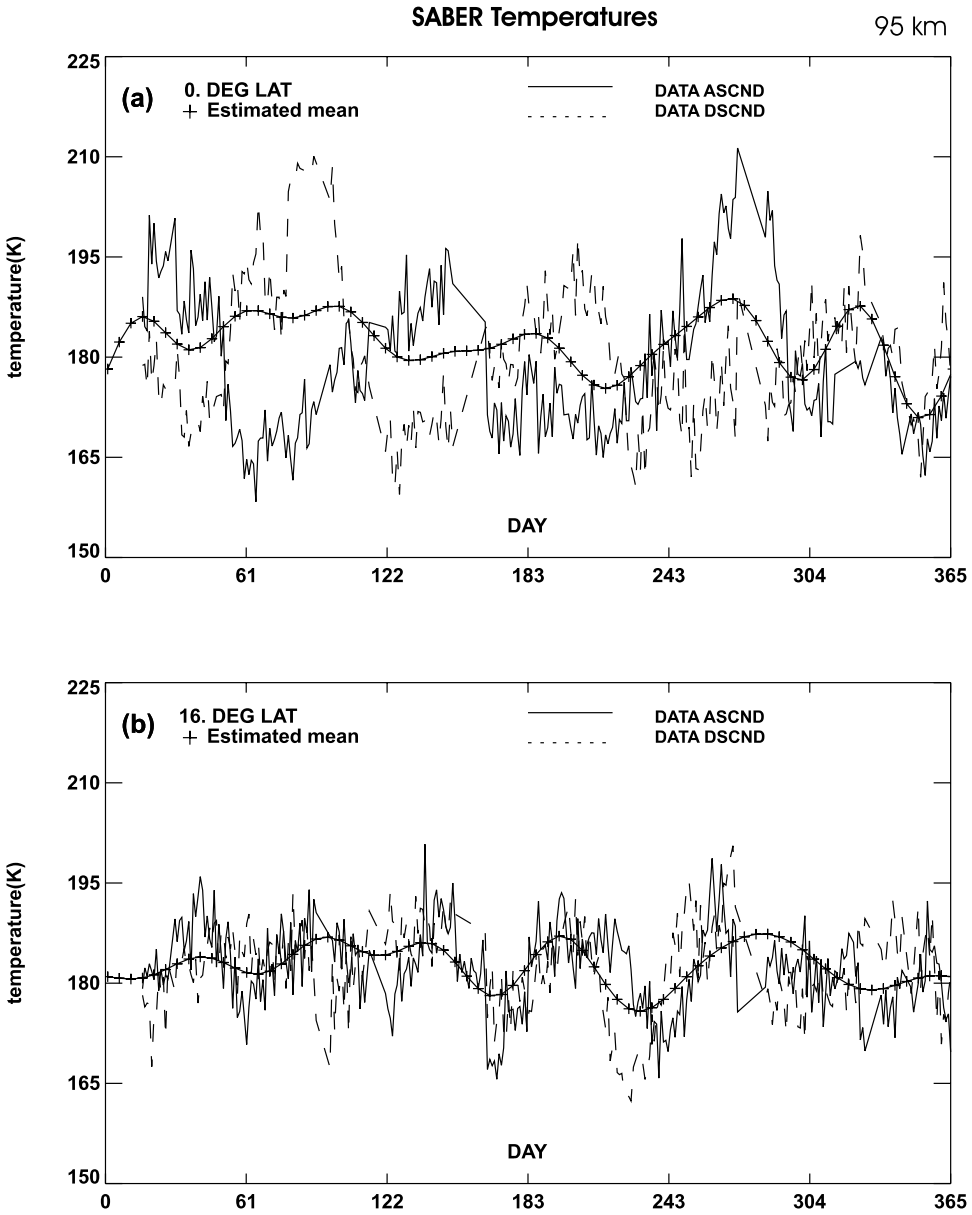

Figure 1. SABER kinetic temperatures averaged over longitude at 95 km, plotted versus day of year (2003) (a) at the equator and (b) at 16°N latitude. Solid and dashed lines represent ascending and descending mode data, respectively, corresponding to two different local times (LST) for each day. (It takes 60 days to sample data over the full range of local times.) Plusses represent the estimated zonal mean values derived with our algorithm.

tides, which are discussed in detail in an accompanying paper [*Huang et al.*, 2006].

2.1.2. Algorithm

[11] With independent variables being local solar time and day of year, the data are described analytically in the form of a two-dimensional Fourier series

$$\Psi(t_l, d, z, \theta) = \sum_n \sum_m b_{nm}(z, \theta) e^{i2\pi n t_l} e^{i2\pi m d/365} \qquad (1)$$

where $\Psi(t_l, d, z, \theta)$ represent the data averaged in longitude around a latitude circle; z is altitude; *d* day of year; θ latitude, *t* time (fraction of a day); t_l local solar time (fraction of a day); $t_l = t + \lambda/(2\pi)$, λ = longitude. It is understood that the summations in equation (1) involve complex and conjugate terms.

[12] The algorithm minimizes the sum of the squares of the differences between the Fourier series (equation (1)) and the data over a 365-day period. Once the coefficients, $\{b_{nm}(z, \theta)\}$, are estimated, both the zonal-mean values and the tidal variations with local time can be calculated directly from equation (1) for a given day of year. More details concerning the algorithm and applications to UARS data are given by *Huang et al.* [1997] and *Huang and Reber* [2001, 2003].

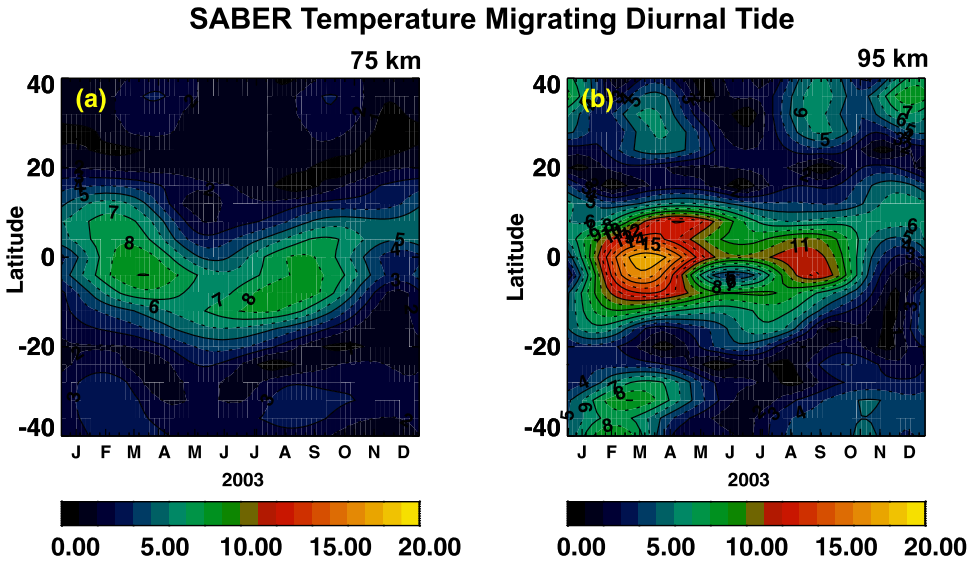

Figure 2. Derived temperature amplitudes from SABER data for diurnal migrating tides at (a) 75 km and (b) 95 km, plotted versus latitude and day of year 2003.

2.2. Numerical Spectral Model (NSM)

[13] The numerical results shown here are taken from a three-dimensional (3-D) study with the Numerical Spectral Model (NSM), which describes the migrating and non-migrating tides in the mesosphere under the influence of parameterized gravity waves [*Mayr et al.*, 2005a, 2005b].

[14] The NSM is integrated from the Earth's surface into the thermosphere at 240 km in the present application. For the zonal mean, the NSM is driven in the mesosphere and stratosphere by solar heating from UV radiation [*Strobel*, 1978] and by EUV radiation in the thermosphere. A zonal-mean heat source in the troposphere qualitatively reproduces the observed zonal circulation and temperature variations near the tropopause. For the migrating tides, the heating rates in the middle atmosphere and troposphere are taken from *Forbes and Garrett* [1979]. The radiative loss is

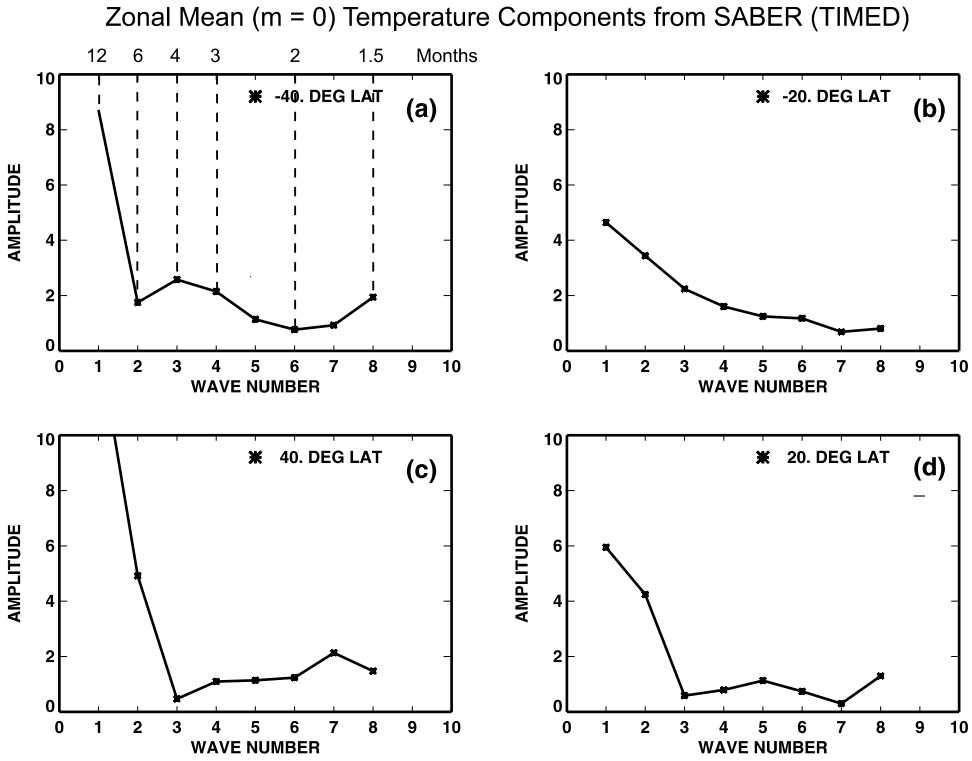

Figure 3. Derived Fourier amplitudes for the zonal mean temperature variations at 75 km, (a) 40°S, (b) 20°S, (c) 40°N, and (d) 20°N, plotted versus wave number (e.g., 1: annual, 2: semiannual, 3: ter-annual, etc). The periods associated with wave numbers are given in Figure 3a.

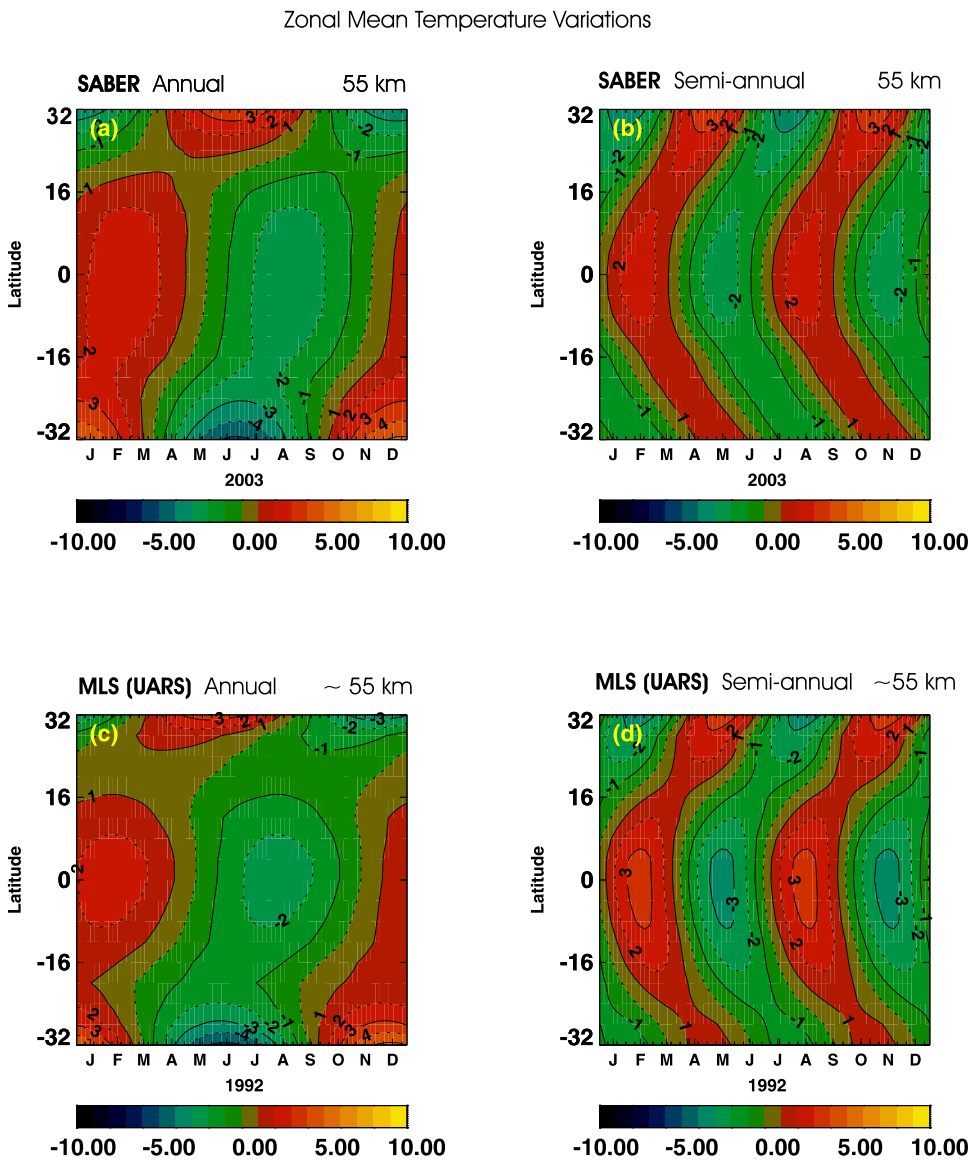

Figure 4. Derived annual and semi-annual temperature components at 55 km plotted versus latitude and day of year. Upper row is from SABER for year 2003; lower row is from MLS (UARS) for year 1992.

described in terms of Newtonian cooling, which is taken from the parameterization of *Zhu* [1989].

[15] An integral part of the NSM is that the model incorporates the Doppler Spread Parameterization (DSP) for small-scale gravity waves (GW) formulated by *Hines* [1997a, 1997b]. The DSP has been extensively discussed in the literature and has been applied successfully in a number of models [e.g., *Akmaev*, 2001; *Manzini et al.*, 1997; *McLandress*, 1998; *Mengel et al.*, 1995]. In the DSP, a spectrum of waves interacts with each other to produce Doppler spreading, which affects the interactions of the waves with the background flow. The GWs are assumed to originate in the troposphere, and the source is isotropic and independent of latitude and season.

[16] The NSM is run with a time step of about 5 min and a vertical step size of 0.5 km (below 120 km) to resolve the GW interactions with the flow. The NSM is truncated at the zonal and meridional wave numbers $m = 4$ and $l = 12$, respectively.

[17] As mentioned earlier, *Mayr et al.* [2003] showed that the NSM generates in the zonal mean (m = 0) meridional wind oscillations with periods similar to those inferred from UARS observations [*Huang et al.*, 2005; *Huang and Reber*, 2003]. *Mayr et al.* [2003] also described the associated temperature oscillations. Numerical experiments, reported in that paper, demonstrated that the modeled meridional wind and temperature oscillations have the properties of a nonlinear auto-oscillator, which is generated by the wave-mean-flow interaction from parameterized GWs propagating in the meridional (north/south) directions. The oscillation thus was considered to be the counterpart to the quasi-biennial oscillation (QBO) in the zonal winds. In contrast to the solenoidal zonal winds for m = 0, the much smaller irrotational (divergent) meridional

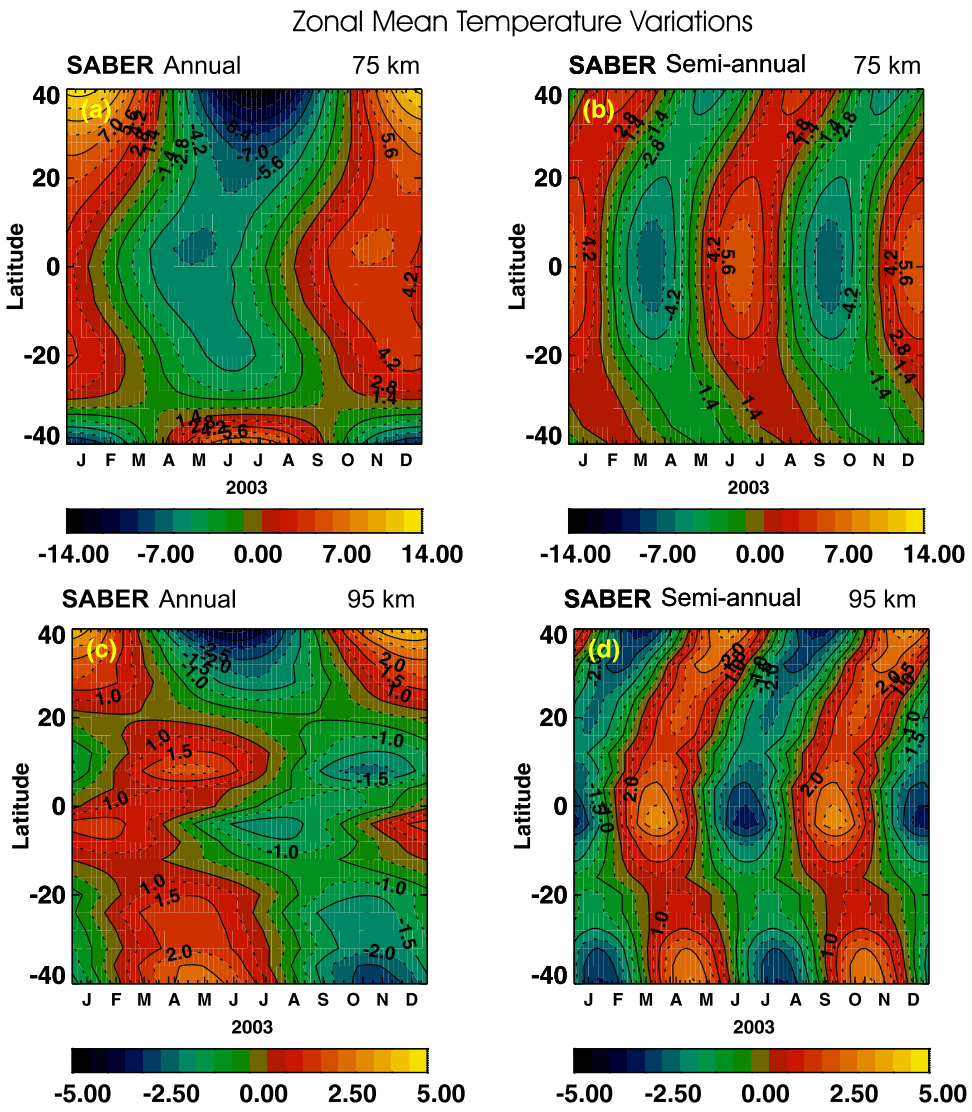

Figure 5. Annual and semiannual Fourier components of zonal mean temperatures for year 2003 derived from SABER data at (top) 75 km and (bottom) 95 km, shown on latitude versus day-of-year coordinates.

winds are damped additionally, and directly, by meridional energy transport and the resulting pressure feedback. With the shorter time constant for dissipation, the resulting oscillation periods for the meridional winds (and temperatures), of order months, are then also shorter than those for the zonal winds of the QBO.

3. Inferred Temperature Variations

3.1. Diurnal and Semidiurnal Tides

[18] As discussed earlier, tides contribute significantly to the observed variations and need to be accounted for in the analysis, in order to assure that the inferred zonal mean values are not biased. With Figure 2, we present examples for the derived temperature of the diurnal migrating tide obtained from SABER data for year 2003 at 75 and 95 km altitudes. Although not shown, we have also estimated semidiurnal tides corresponding to diurnal tides. More tidal results based on TIMED data are given by *Huang et al.* [2006].

[19] The diurnal variations that have been studied are based mainly on wind measurements. As noted by *Forbes* [1984], there are average tidal structures that cover periods of a month or more, and deviations from the average have periods from a few days to a month. *Vial* [1989] noted that monthly averages are more appropriate in the climatological sense. Since it takes 60 (36) days to sample the full range of local times for TIMED (UARS), our empirical model cannot produce the short-term variations with periods of a few days. The short-term variations are thus smoothed out, but the above SABER data provide enough information (coefficients) to describe the underlying trend of the annual and semiannual tidal variability.

3.2. Zonal Mean

[20] On the basis of SABER data at 75 km, we present in Figure 3 for the zonal mean the derived Fourier amplitudes as a function of wave number (relative to the annual cycle). In Figure 3a, the periods are given versus wave number

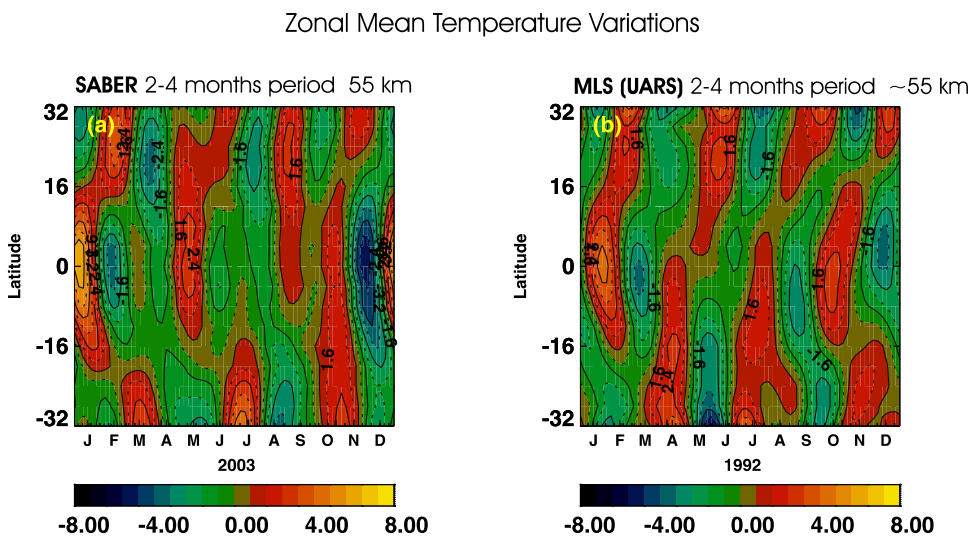

Figure 6. Zonal mean Fourier components with periods between 2 and 4 months on latitude versus day of year coordinates. (left) Derived results based on SABER data at 55 km, year 2003 and (right) based on MLS data at 55 km, year 1992.

(e.g., 1 for the annual harmonic, 2 the semiannual, 3 the terannual). Beginning clockwise from the top left, the amplitudes are given at 40°S, 20°S, 20°N, and 40°N, respectively. It can be seen that the amplitudes corresponding to wave numbers 3 to 8 (4 to 1.5-month periods) are not negligible compared to the semiannual component. The latitudinal and day of year variations for the individual harmonics are presented in the next figures. We note that the uncertainties in the amplitudes are uniformly about 0.1°K or less, but they do not include consideration of uncertainties in the individual data points. The small values of the uncertainties reflect the adequate temporal and spatial coverage of the data.

[21] In Figure 4 we show the annual and semiannual components of zonal mean temperatures at 55 km derived from SABER (top) and MLS (bottom) data, plotted on latitude and day of year coordinates. The two seasonal components derived from SABER for year 2003 and MLS for 1992 are in substantial agreement. The phase shifts in the annual component (Figure 4a) near 20°N for SABER and MLS, indicative of hemispherical asymmetry, are also in qualitative agreement with *Remsberg et al.* [2002] based on data from the Halogen Occultation Experiment (HALOE) on UARS, and with *Fleming et al.* [1988, 1990] based on data from a variety of sources spanning several decades.

[22] Corresponding to Figure 4, we present in Figure 5 for year 2003 the annual and semiannual components of the temperatures derived from SABER data at 75 km (top row) and 95 km (bottom row). At 75 km, the phase shifts of the

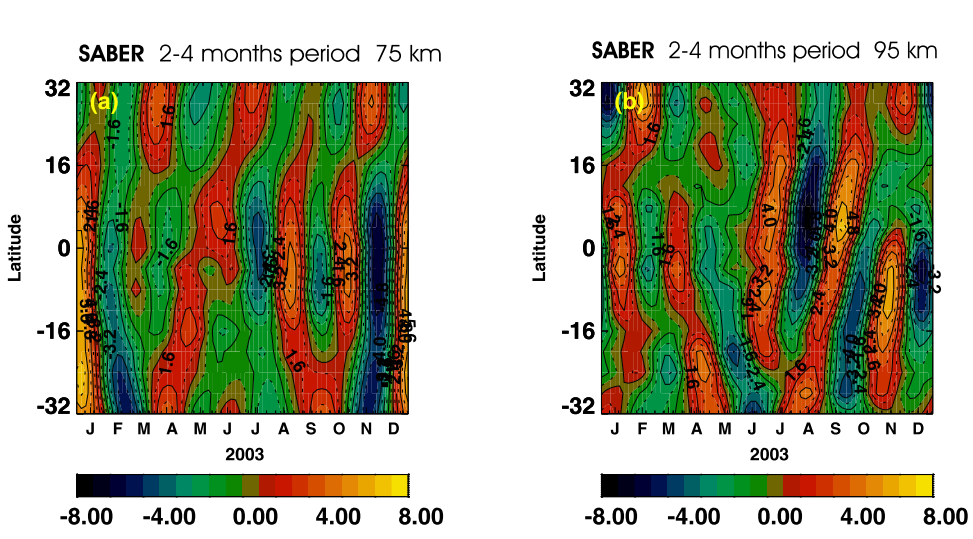

Figure 7. Zonal mean Fourier components with periods between 2 and 4 months on latitude versus day of year coordinates, based on SABER data for year 2003 obtained at (a) 75 km and (b) 95 km.

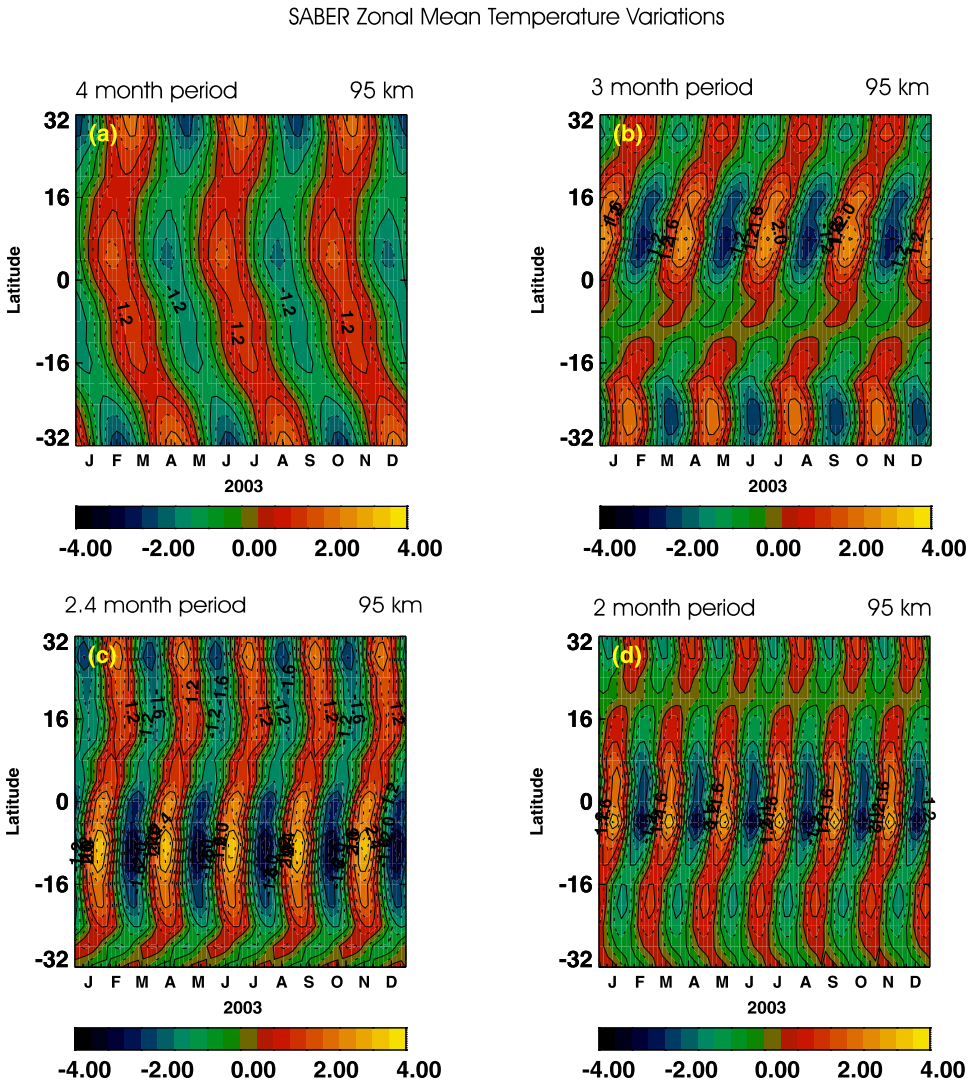

Figure 8. Individual Fourier components of mean temperatures derived from SABER data at 95 km, year 2003 on latitude versus day of year coordinates. Top left, top right, bottom left, and bottom right plots correspond to periods of 4, 3, 2.4, and 2 months, respectively.

annual component near 30°S are qualitatively consistent with those shown by *Remsberg et al.* [2002] and *Fleming et al.* [1988, 1990]. The phase variations for the semiannual component at 75 km agree more with those of Remsberg et al. than with those of Fleming et al.

[23] With Figure 6 we present the zonal mean temperature variations reconstructed from Fourier components for periods between 2 and 4 months, again plotted on latitude versus day-of-year coordinates. The results are based on data from SABER (Figure 6a) at 55 km for year 2003 and from MLS (Figure 6b) at about 55 km for year 1992. The inferred oscillation patterns from SABER and MLS reveal similarities and comparable amplitudes. In both data sets, pronounced asymmetries are apparent between the northern and southern hemispheres, though usually not centered at the equator. Hemispherical asymmetries are expected if the temperature oscillations are generated by dynamical heating and cooling associated with meridional winds across the equator. Interannual variations may in part account for the differences between the SABER and MLS results, which are derived from data sampled almost 10 years apart.

[24] Figure 7 corresponds to Figure 6, but is based on SABER data at 75 km (Figure 7a) and 95 km (Figure 7b). In addition to the above mentioned phase differences between the two hemispheres, the results show that there are phase differences as a function of altitude at 55, 75, and 95 km. The oscillations at 55 km and 95 km have almost opposite phase, and there are significant phase shifts between 75 and 95 km as well. These types of phase variations with altitude are qualitatively consistent with the results from the NSM.

[25] Corresponding to Figure 7b, individual Fourier components of the zonal mean temperature variations at 95 km are shown in Figure 8 for the periods between 2 and 4 months. The amplitudes have comparable magnitudes close to 2 K, and the phase variations with latitude are pronounced.

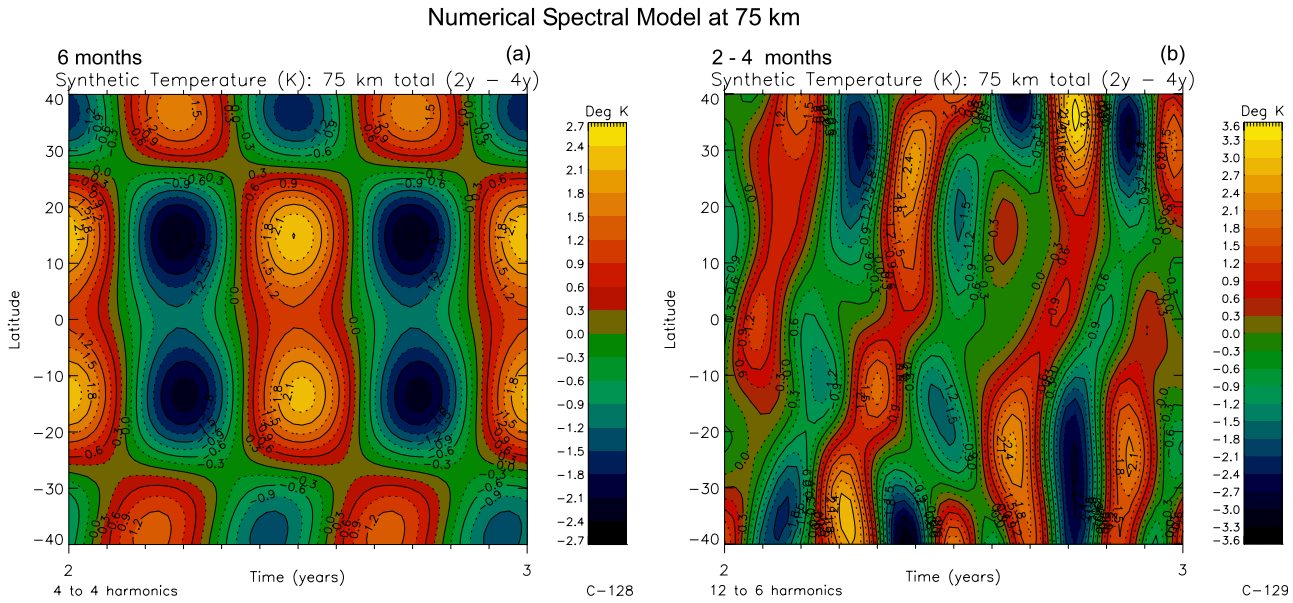

Figure 9. Temperature variations versus latitude at 75 km from the NSM covering 2 to 4 years. (a) Semiannual (6-month) component, (b) periods from 2 to 4 months. The oscillations are computed from Fourier analysis for the 2-year time span of the model run, but the synthesized results are shown only for 1 year, which is sufficient to reveal the characteristics. While the semiannual component is induced by the seasonal cycle, its amplitude is affected significantly by wave interaction. The short-period oscillations are believed to be generated primarily by gravity waves propagating in the north/south

[26] For comparison, we present with Figure 9 some results for the zonal-mean temperature variations at 75 km taken from the NSM [*Mayr et al.*, 2005a, 2005b]. Plotted on latitude versus time of year coordinates, we show the computed oscillations for (Figure 9a) periods of 6 months (semiannual) and (Figure 9b) from 2 to 4 months. The results are obtained from a Fourier analysis of model results covering the time span from 2 to 4 years. However, the synthesized results are only presented for 1 year, which is sufficient to characterize the oscillations. Around the equator and at 75 km, the semiannual temperature oscillation in the model is in phase with the observations shown in Figure 5. At 55 and 95 km (not shown), the phase from the NSM also agrees with the observations. As seen from Figure 9, however, the computed amplitude for the semiannual oscillation is significantly smaller than that inferred from the SABER observations. This discrepancy brings to light a problem with the current version of the NSM, which needs to be upgraded apparently in its treatment of the equatorial waves that largely control the semiannual oscillation. Trial runs show that the semiannual variations in the zonal winds and temperature are affected significantly by such factors as the adopted latitude dependence of the gravity wave source and the altitude in the troposphere where the gravity waves originate. Equatorially trapped planetary waves, not presently incorporated, could also be important for the semiannual oscillation in the stratosphere.

[27] The NSM reproduces qualitatively the observed pattern in the intraannual variations with periods between 2 and 4 month shown in Figure 9b. The amplitudes are comparable to those observed in Figure 7a, and the asymmetries between the northern and southern hemispheres are also apparent. In the NSM, the intra-seasonal oscillations are generated in part by wave mean flow interactions. This was shown by *Mayr et al.* [2003] where the north-south propagating gravity waves were identified as a source. However, nonlinear interactions between the annual and semiannual oscillations may also be involved, and the intraseasonal harmonics of the solar heating rates could also contribute. As is the case for the semiannual oscillation, the differences between the NSM and the SABER results are likely related to the uncertainties in the applied wave source. Interannual variations associated with the QBO would also contribute.

[28] The analysis and comparison of results over multiple years and a full range of altitudes would help characterize the variability of the empirical results. Additional runs of the NSM will help to determine the degree of agreement that can be reached between the NSM and the empirical results.

4. Summary and Conclusion

[29] We have derived the variations of the zonal mean temperatures based on SABER (TIMED) data and compared them with corresponding results from MLS (UARS) and from the Numerical Spectral Model (NSM). The variations are presented in the form of Fourier harmonics over an annual cycle, and the focus is on periods from 2 to 4 months. Although the UARS and TIMED data were taken about 10 years apart, the SABER and MLS results agree in general quite well. The variations with periods from 2 to 4 months are mostly out of phase in the northern and southern hemispheres, but they are not centered at the equator. Corresponding results from the NSM also show

these phase differences in temperature between the hemispheres. In details, there is not quantitative agreement between the temperature variations inferred from MLS and SABER and with the NSM. This is not unexpected considering the interannual variations that are known to occur even between the MLS results based on 1992 and 1993 data (not shown), and the SABER data were from 2003. In the NSM run presented [*Mayr et al.*, 2005a, 2005b], a relatively weak QBO is generated with a source of small-scale gravity waves that was assumed to be independent of latitude and season, and the model was not tuned in any way to simulate the observations. The analysis and comparison of results over multiple years and a full range of altitudes will be needed to fully characterize the observed (empirically inferred) variability, and additional runs of the NSM will be required either to better match the observations or, alternatively, identify some problems in our understanding.

[30] The above-discussed temperature results for oscillations with periods between 2 and 4 months are qualitatively consistent with the existence of mean meridional flows across the equator with similar periods. Such oscillations have been inferred from UARS measurements [*Huang et al.*, 2005; *Huang and Reber*, 2003] and were predicted with the NSM [*Mayr et al.*, 2003]. Given these oscillations across the equator, the resulting dynamical heating or cooling should produce temperature oscillations with opposite phase in the northern and southern hemispheres, depending on the convergence or divergence of the meridional flow, respectively. While the temperature oscillations in Figures 6 to 8 do not vanish at the equator in general, nodes appear close to the equator, and the temperature variations in the opposing hemispheres tend to be in opposite phase. In contrast to the meridional wind oscillations, which are in phase at any given time during the year in the two hemispheres, the temperature oscillations are distinctively "slanted or sloping." Thus there is circumstantial evidence that the temperature oscillations could be driven by the meridional winds, which in turn could be generated by wave interactions.

[31] To help corroborate the relatively small temperature variations of a few degrees or less that characterize the above-discussed intraseasonal oscillations, *Huang et al.* [2005] analyzed the ozone mixing ratios that are measured simultaneously by the MLS instrument on UARS. At altitudes above about 45 km, the ozone chemistry dominates over dynamics, and it is expected that the variations in the mean ozone and temperature are anticorrelated [*Hartmann and Garcia*, 1978; *Rood and Douglass*, 1985]. As shown by *Huang et al.* [2005], such anticorrelations are indeed observed for the oscillations with the periods between 2 and 4 months that are discussed in the present paper. At lower altitudes, chemical reactions become less important so that the temperature and ozone variations tend to be in phase.

[32] **Acknowledgments.** We thank two anonymous reviewers for their insightful and helpful comments.

[33] Lou-Chuang Lee thanks the reviewers for their assistance in evaluating this paper.

References

Akmaev, R. A. (2001), Simulation of large-scale dynamics in the mesosphere and lower thermosphere with the Doppler-spread parameterization of gravity waves 1 implementation and zonal mean climatologies, *J. Geophys. Res.*, *106*, 1193–1204.

Barath, F. T., et al. (1993), The Upper Atmosphere Research Satellite Microwave Limb Sounder Instrument, *J. Geophys. Res.*, *98*, 10,751–10,762.

Beig, G., et al. (2003), Review of mesospheric temperature trends, *Rev. Geophys.*, *41*(4), 1015, doi:10.1029/2002RG000121.

Eckermann, S. D., D. K. Rajopadhyaya, and R. A. Vincent (1997), Intraseasonal wind variability in the equatorial mesosphere and lower thermosphere: Long-term observations from the central Pacific, *J. Atmos. Sol. Terr. Phys.*, *59*, 603–627.

Fleming, E. L., S. Chandra, M. R. Schoeberl, and J. J. Barnett (1988), Monthly mean global climatology of temperature, wind, geopotential height, and pressure for 0–120 km, *NASA Tech. Memo.*, *100697*, 1–85.

Fleming, E. L., S. Chandra, J. J. Barnett, and M. Corney (1990), Zonal mean temperature, pressure, zonal wind and geopotential height as functions of latitude, *Adv. Space Res.*, *10*, (12)11–(12)59.

Forbes, J. M. (1984), Middle atmosphere tides, *J. Atmos. Terr. Phys.*, *46*, 1049–1067.

Forbes, J. M., and H. B. Garrett (1979), Theoretical studies of atmospheric tides, *Rev. Geophys.*, *17*, 1951–1981.

Forbes, J. M., M. Kilpatrick, D. Frits, A. H. Manson, and R. A. Vincent (1997), Zonal mean and tidal dynamics from space: An empirical examination of aliasing and sampling issues, *Ann. Geophys.*, *15*, 1158–1164.

Hartmann, D. L., and R. R. Garcia (1978), A mechanistic model of ozone transport by planetary waves in the stratosphere, *J. Atmos. Sci.*, *36*, 350–364.

Hays, P. B., V. J. Abreu, M. E. Dobbs, D. A. Gell, H. J. Grassl, and W. B. Skinner (1993), The High Resolution Doppler Imager on the Upper Atmosphere Research Satellite, *J. Geophys. Res.*, *98*, 10,713–10,723.

Hines, C. O. (1997a), Doppler-spread parameterization of gravity-wave momentum deposition in the middle atmosphere, 1, Basic formulation, *J. Atmos. Sol. Terr. Phys.*, *59*, 371.

Hines, C. O. (1997b), Doppler-spread parameterization of gravity-wave momentum deposition in the middle atmosphere, 2, Broad and quasi monochromatic spectra, and implementation, *J. Atmos. Sol. Terr. Phys.*, *59*, 387.

Huang, F. T., and C. A. Reber (2001), "Synoptic" estimates of chemically active species and other diurnally varying parameters in the stratosphere, derived from measurements from the Upper Atmosphere Research Satellite (UARS), *J. Geophys. Res.*, *106*, 1655–1667.

Huang, F. T., and C. A. Reber (2003), Seasonal behavior of the semidiurnal and diurnal tides, and mean flows at 95 km, based on measurements from the High Resolution Doppler Imager (HRDI) on the Upper Atmosphere Research Satellite (UARS), *J. Geophys. Res.*, *108*(D12), 4360, doi:10.1029/2002JD003189.

Huang, F. T., C. A. Reber, and J. Austin (1997), Ozone diurnal variations observed by UARS and their model simulation, *J. Geophys. Res.*, *102*, 12,971–12,985.

Huang, F. T., H. G. Mayr, and C. A. Reber (2005), Intra-seasonal Oscillations (ISO) of zonal-mean meridional winds and temperatures as measured by UARS, *Ann. Geophys.*, *23*, 1131–1137.

Huang, F. T., H. G. Mayr, C. A. Reber, T. Killeen, J. Russell, M. Mylnczak, W. Skinner, and J. Mengel (2006), Diurnal variations of temperature and winds inferred from TIMED and UARS measurements, *J. Geophys. Res.*, doi:10.1029/2005JA011426, in press.

Lieberman, R. S. (1998), Intraseasonal variability of high resolution Doppler imager winds in the equatorial mesosphere and lower thermosphere, *J. Geophys. Res.*, *103*, 11,221–12,228.

Manzini, E., N. A. McFarlane, and C. McLandress (1997), Impact of the Doppler spread parameterization in the simulation of the middle atmosphere circulation using the MA/ECHAM4 general circulation model, *J. Geophys. Res.*, *102*, 25,751.

Mayr, H. G., J. G. Mengel, D. P. Drob, H. S. Porter, and K. L. Chan (2003), Intra-seasonal oscillations in the middle atmosphere forced by gravity waves, *J. Atmos. Sol. Terr. Phys.*, *65*, 1187–1203.

Mayr, H. G., J. G. Mengel, E. R. Talaat, H. S. Porter, and K. L. Chan (2005a), Mesospheric non-migrating tides generated with planetary waves: I. Characteristics, *J. Atmos. Sol. Terr. Phys.*, *67*, 959.

Mayr, H. G., J. G. Mengel, E. R. Talaat, H. S. Porter, and K. L. Chan (2005b), Mesospheric non-migrating tides generated with planetary waves: II. Influence of gravity waves, *J. Atmos. Sol. Terr. Phys.*, *67*, 981.

McLandress, C. (1998), On the importance of gravity waves in the middle atmosphere and their parameterization in general circulation models, *J. Atmos. Sol. Terr.*, *60*(14), 1357–1383.

Mengel, J. G., H. G. Mayr, K. L. Chan, C. O. Hines, C. A. Reddy, N. F. Arnold, and H. S. Porter (1995), Equatorial oscillations in the middle atmosphere generated by small scale gravity waves, *Geophys. Res. Lett.*, *22*, 3027.

Reber, C. A. (1993), The Upper Atmosphere Research Satellite (UARS), *Geophys. Res. Lett.*, *20*(12), 1215–1218.

Remsberg, E. E., P. P. Bhatt, and L. E. Deaver (2002), Seasonal and longer-term variations in middle atmosphere temperature from HALOE on UARS, *J. Geophys. Res.*, *107*(D19), 4411, doi:10.1029/2001JD001366.

Roche, A. E., J. B. Kumer, J. L. Mergenthaler, G. A. Ely, W. G. Uplinger, J. F. Potter, T. C. James, and L. W. Sterritt (1993), The Cryogenic Limb Array Etalon Spectrometer (CLAES) on UARS: Experiment description and performance, *J. Geophys. Res.*, *98*, 10,763–10,775.

Rood, R. B., and A. Douglass (1985), Interpretation of ozone temperature correlations: 1. Theory, *J. Geophys. Res.*, *90*, 5733–5743.

Russell, J. M., III, M. G. Mlynczak, L. L. Gordley, J. Tansock, and R. Esplin (1999), An overview of the SABER experiment and preliminary calibration results, *Proc. SPIE*, *3756*, 277–288.

Strobel, D. F. (1978), Parameterization of atmospheric heating rate from 15 to 120 km due to O2 and O3 absorption of solar radiation, *J. Geophys. Res.*, *83*, 7963.

Vial, F. (1989), Tides in the middle atmosphere, *J. Atmos. Terr. Phys.*, *51*, 3–17.

Zhu, X. (1989), Radiative cooling calculated by random bans models with S-1-beta tailed distribution, *J. Atmos. Sci.*, *46*, 511.

F. T. Huang, Creative Computing Solutions Inc., Rockville, MD 20850, USA. (fthuang@comcast.net)

H. G. Mayr and C. A. Reber, NASA Goddard Space Flight Center, Greenbelt, MD 20771, USA.

J. Mengel, Science Systems and Applications, Lanham, MD 20706, USA.

M. Mlynczak, NASA Langley Research Center, Hampton, VA 23681, USA.

J. Russell, Center for Atmospheric Sciences, Hampton University, Hampton, VA 23668, USA.